

Supporting information

High-performance fuel cell designed for coking-resistance and efficient conversion of waste methane to electrical energy

Tao Li¹, Xuekun Lu², Mohamad F. Rabuni^{1,4}, Bo Wang¹, Nicholas M. Farandos³, Geoff H. Kelsall³, Dan J. L. Brett², Paul R. Shearing², Mengzheng Ouyang⁵, Nigel P. Brandon⁵ and Kang Li^{1*}

¹ Barrer Center, Department of Chemical Engineering, Imperial College London, London SW7 2AZ, UK

² Electrochemical Innovation Lab, Department of Chemical Engineering, University College London, London WC1E 7JE, UK

³ Department of Chemical Engineering, Imperial College London, London SW7 2AZ, UK

⁴ Department of Chemical Engineering, University of Malaya, 50603 Kuala Lumpur, Malaysia

⁵ Department of Earth Science and Engineering, Imperial College London, London SW7 2AZ, UK

Method

Preparation of micro-monolithic ceramic fuel cell

The 6-channel, micro-monolithic anode support was prepared via a phase inversion-assisted extrusion technique (Supplementary Fig. 1), the details of which have been described elsewhere ²⁰.

Yttria-stabilized zirconia (8 mol% YSZ), gadolinium-doped ceria (10 mol% GDC), nickel oxide (NiO) and lanthanum strontium cobalt ferrite ($\text{La}_{0.6}\text{Sr}_{0.4}\text{Co}_{0.2}\text{Fe}_{0.8}\text{O}_{3-\delta}$, LSCF) were purchased from Fuel Cell Materials (USA) and used as supplied. Poly (methyl methacrylate) (Acrypet-PMMA, Mitsubishi Rayon Co. Ltd), 30-dipolyhydroxystearate (Arlacel P135, Uniqema), and N-methyl-2-pyrrolidone (NMP, HPLC grade, VWR) were applied as the polymer binder, dispersant and solvent, respectively. The mixture of deionized (DI) water and ethanol (VWR International) was used as internal coagulant.

Generally, ceramic powders, solvent and organic additives were mixed and ball-milled (SFM-1 Desktop Miller, MTI Corporation, USA) for 4 days to obtain a homogeneous spinning suspension, which was latter degassed under vacuum to eliminate air bubbles prior to the extrusion process. The extrusion rates of various components were precisely controlled by syringe pumps (Harvard

PHD22/200 HPsi). A weight ratio of 70/30 was selected for the water-ethanol internal coagulant to ensure the optimized morphology in the resultant anode precursor, which was subsequently dried and straightened at room temperature.

YSZ-GDC dual-layer electrolyte was dip-coated onto the anode precursor, while preventing it accessing the channels in the anode by sealing using PTFE film. After both layers of electrolyte coating were dried, they were co-sintered at 1400 °C in ambient air for 6 hours. Finally, the LSCF-GDC cathode with a length of 10 mm was dip-coated onto the sintered half-cell that had been cut to a length of 50 mm and subsequently sintered at 1000 °C for 1 h. The thickness of the cathode layer was approximately 25 µm.

X-ray computed tomography

Non-destructive X-ray computed tomographic imaging of the fabricated micro-monolithic anode was conducted on a Zeiss Xradia Versa 520 X-ray microscope at the Electrochemical Innovation Lab (EIL), University College London. 2001 X-ray projections with a voxel size of 1.55 µm were collected with an exposure time of 18 seconds during the angular rotation of 360 degrees. These radiographic projections were then reconstructed by a proprietary Feldkamp-Davis-Kress (FDK) algorithm in the Zeiss Xradia XMReconstructor software. Post-processing of the reconstructed CT data was conducted using Avizo 9.4 (Thermo Fisher Scientific, UK).

Computational fluid dynamics (CFD) simulation

The reconstructed 3D volume of the monolithic anode was firstly segmented into solid and pore phases using standard thresholding method based on the grayscale difference. A 260 µm thick disc with half of the geometry was then meshed and imported into the commercial CFD software Star CCM+ (CD-adapco Inc., London) for image-based simulation. Two types of inlet boundary conditions were set: pure H₂ and 20 % H₂ + 80 % inert diluent to compare the mass transport performance at different operating conditions. At the outlet, a negative source flux corresponding to the current density of 1, 2 and 4 A cm⁻² was set respectively to mimic the consumption of reactants at the EAR

near the electrode/electrolyte interface. In a porous electrode, the molar flux density can be expressed by the modified Fick's law, exemplified in 1D as:

$$J_{H_2} = -\frac{\varepsilon}{\tau} D \frac{dC}{dx} \quad (S1)$$

where J_{H_2} represents the hydrogen molar flux density ($\text{mol m}^{-2} \text{s}^{-1}$), ε and τ the porosity and tortuosity factor, D the diffusion coefficient, C the local concentration (mol m^{-3}), and x the coordinate along permeate direction (m). The CT-resolved micro-channels were modelled as the fluid domain and the solid phase was modelled as the porous medium, with the porosity (29.2 %) and tortuosity factor (8.9) taken from previous measurements ²¹.

Morphological and electrochemical characterizations

The morphology of the micro-monolithic cell was determined using field-emission scanning electron microscopy (FE-SEM, Gemini LEO 1525) under secondary electrons imaging (SEI) mode.

Prior to the electrochemical experiments, current collectors were applied by wrapping silver wires (0.25 mm diameter, 99.99 % purity, Advent Materials Ltd, UK) along the cathode and on the exposed part of the anode. Silver paste was employed to enhance the electric contact between wires and electrode surfaces. A complete single cell with a typical length of 50 mm was then sealed into alumina support tubes with ceramic sealant (Aremco Ceramic Sealant 552, USA) to construct a complete reactor. Wires from both electrodes were connected to a PGSTAT302 N potentiostat with Nova 1.10.2 software (Metrohm Autolab B.V., Netherlands). The base case study was conducted between 650-800 °C, with 50 $\text{cm}^3 \text{min}^{-1}$ of dry H_2 fuel fed to the anode and ambient air to the cathode. For measurements with simulated LCVGs, dry hydrogen was replaced by a mixture of CH_4 and CO_2 (total flow rate 50 $\text{cm}^3 \text{min}^{-1}$, CH_4 concentration of 10, 15 and 20 %). Electrochemical impedance spectroscopy (EIS, 10 mV p-p amplitude) was conducted under open-circuit conditions over the frequency range of 10^5 - 10^{-2} Hz.

Techno-economic evaluation

Outline: The techno-economic analysis was conducted using a model developed previously [1]. In general, various types of costs, including the fixed cost (capital expenditure (CAPEX), auxiliary equipment, maintenance) and operating expenditure (OPEX) (reactant cost, heating and electrical energy input) were estimated together with the profit of generated electricity. To achieve a profitable operation, an electricity price threshold should be first determined, at which the revenue generated from electricity sales will exceed the costs of running the plant.

Plant overview: There are various sources of LCVGs. For example, the Natuna field in Indonesia is the largest gas field in south Asia, with approximately 1.2 trillion cubic metres of reserves and CO₂ content up to 87 % [Journal of Natural Gas Chemistry 21(2012)7–10]. The daily production rate of an exemplar natural gas well is set at 2 million metric cubic feet (MMCF) in this model.

Supplementary Figure S2 shows the proposed plant layout for using LCVGs as the fuel in a ceramic fuel cell (without external reformer). Plant specifications, operating conditions and assumptions are outlined in Supplementary Table S2.

Capital equipment costing: The ceramic fuel cell stack was sized based on its 'reacted' LCVG molar throughput of 6.32 kmol hr⁻¹ resulting in a required reactor area ($A_{reactor}$, m²) of 135.5 m² using equation (S2),

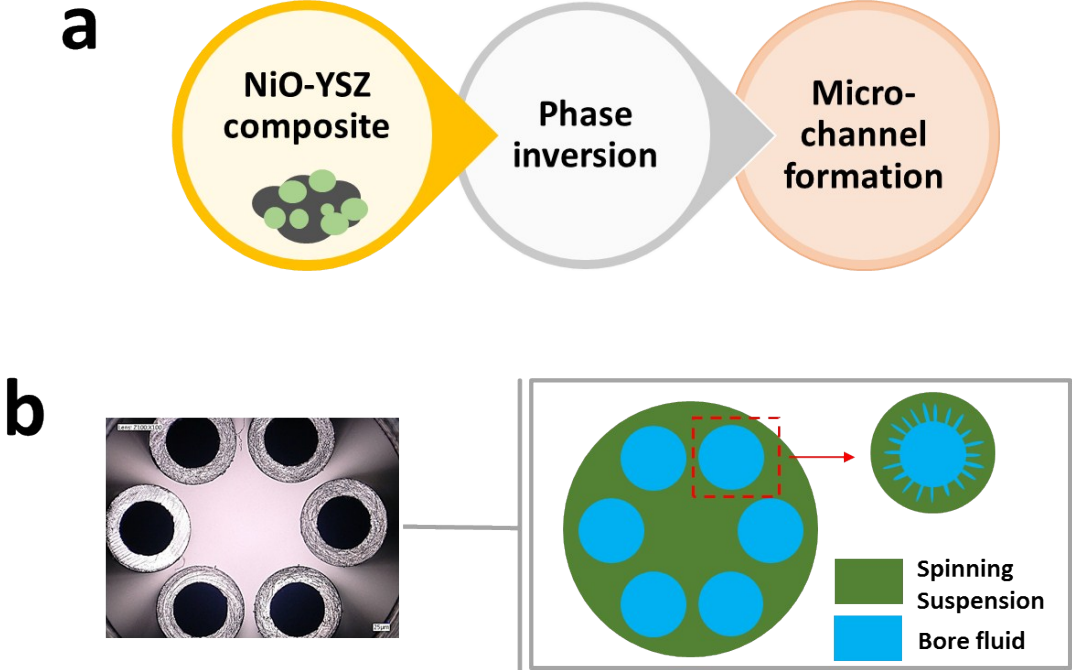
$$A_{reactor} = 8F \frac{dn}{dt} \times \frac{1}{j} \quad (S2)$$

where F is the Faraday's constant (96485 s A mol⁻¹), dn/dt is the molar flow rates and j the current density of the cell.

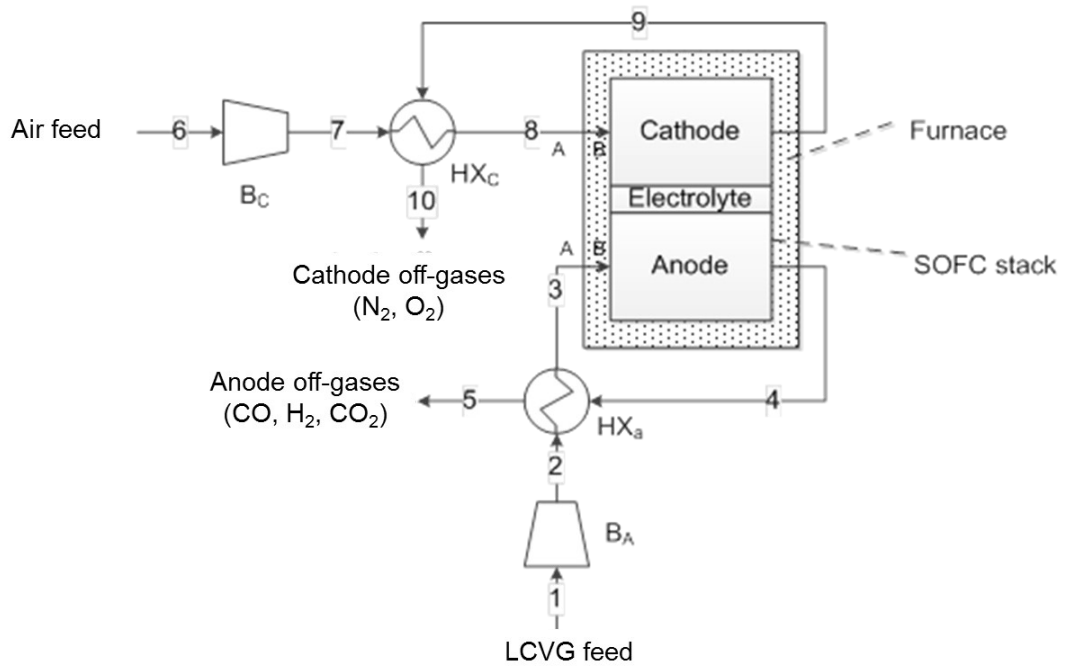
The purchase cost of equipment that is industrially available (i.e. blowers, heat exchangers and furnace) was determined using cost correlations [3, 4]. The blowers (B_A and B_C , where A and C denote the anode and cathode side, respectively) were sized according to the volumetric flow rates of fuel and oxidants. The cost of ceramic fuel cell stack was estimated by doubling the material cost. The mass of individual component, including yttria-stabilised zirconia (YSZ), nickel oxide, gadolinium-doped ceria (GDC) and lanthanum strontium cobalt ferrite (LSCF), was calculated based on the dimensions shown in Figure 1. Silver wires were selected to estimate the cost of current collector (0.25 mm diameter). Using raw material prices of 71.6 \$ kg⁻¹, 1500 \$ kg⁻¹, 1000 \$ kg⁻¹, 74 \$ kg⁻¹ and 0.245 \$ m⁻¹ for YSZ, GDC, LSCF, NiO and silver wire respectively [5], the costs for SOFC stack manufacture were estimated to be ca. \$ 4100 m⁻². CAPEX for all units installed was estimated using Hand Factors (multiplying factor applied to the purchase costs), which are 2.5, 3.5, 2.5 and 2.0 for fuel cell, heat exchangers, blowers and furnaces, respectively [3]. Thus, operating for 7500 years over 10 years, the capital expenditure (CAPEX) per tonne of LCVG was ca. \$ 8.2, 69% of the CAPEX were associated with the fuel cell stack.

Determining operating expenditure (OPEX): Maintenance cost was set at 10% of the CAPEX [6]; hence, \$ 0.95 per tonne of LCVG. Energy required for fuel/oxidant blowers and furnaces were estimated based on the change in specific heat of the streams per hour. Assumption was made that unreacted effluent from anode (CO, H₂ and CO₂) to be burnt to provide energy that maintains furnace temperature. The price of oxidant (compressed air) is \$ 0.02 per cubic meters.

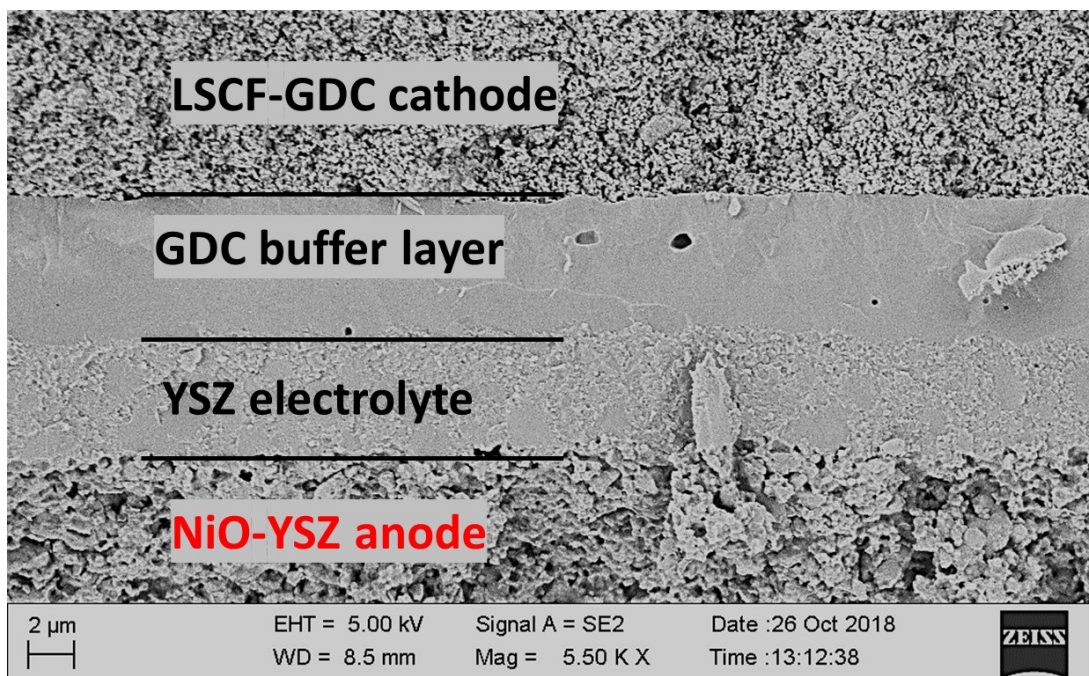
Supplementary figures



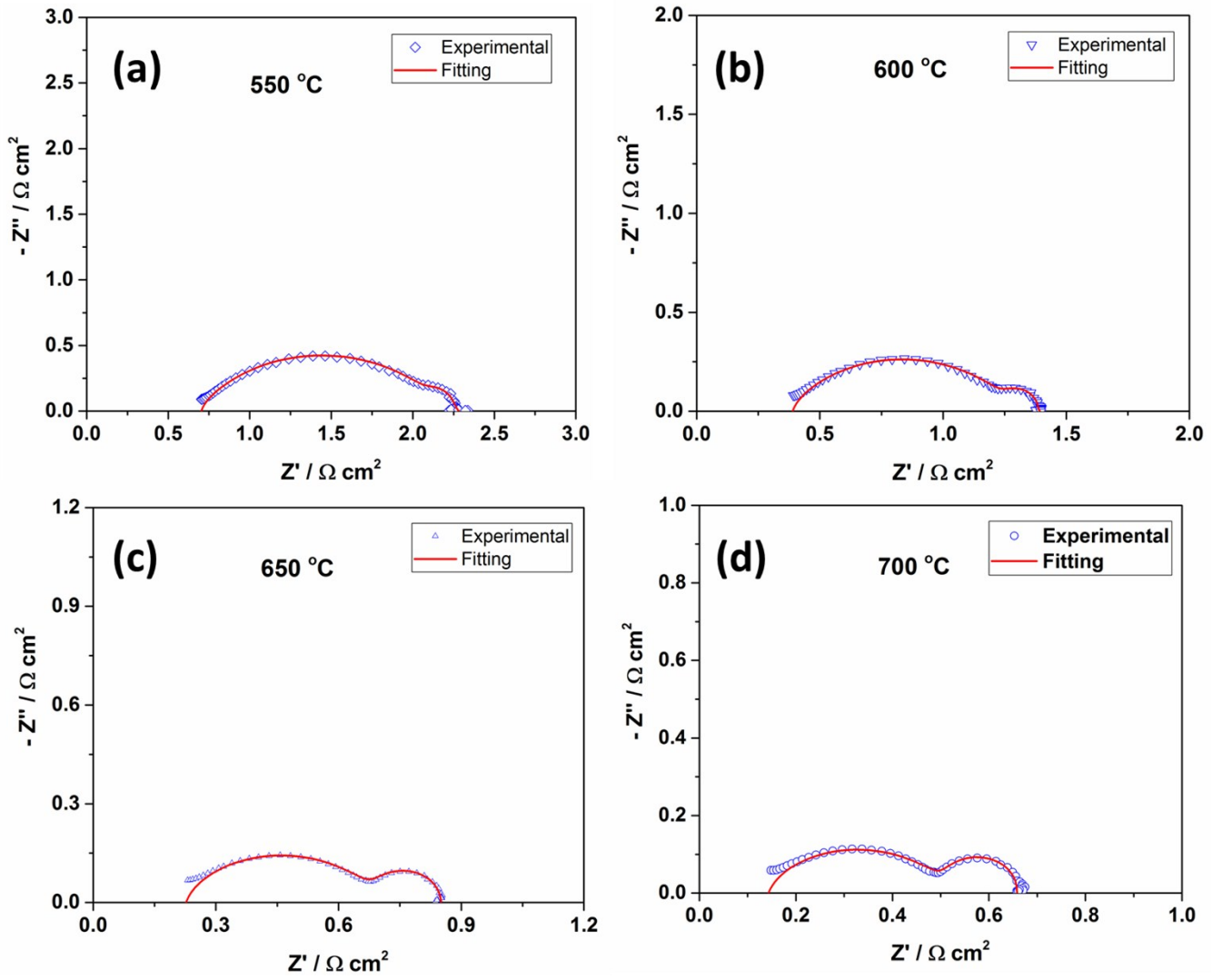
Supplementary Figure 1. **a** schematic diagram of the fabrication procedure of micro-monolithic anode support; **b** optical microscope image of 6-nozzle spinneret and the formation of micro-channels during phase inversion.



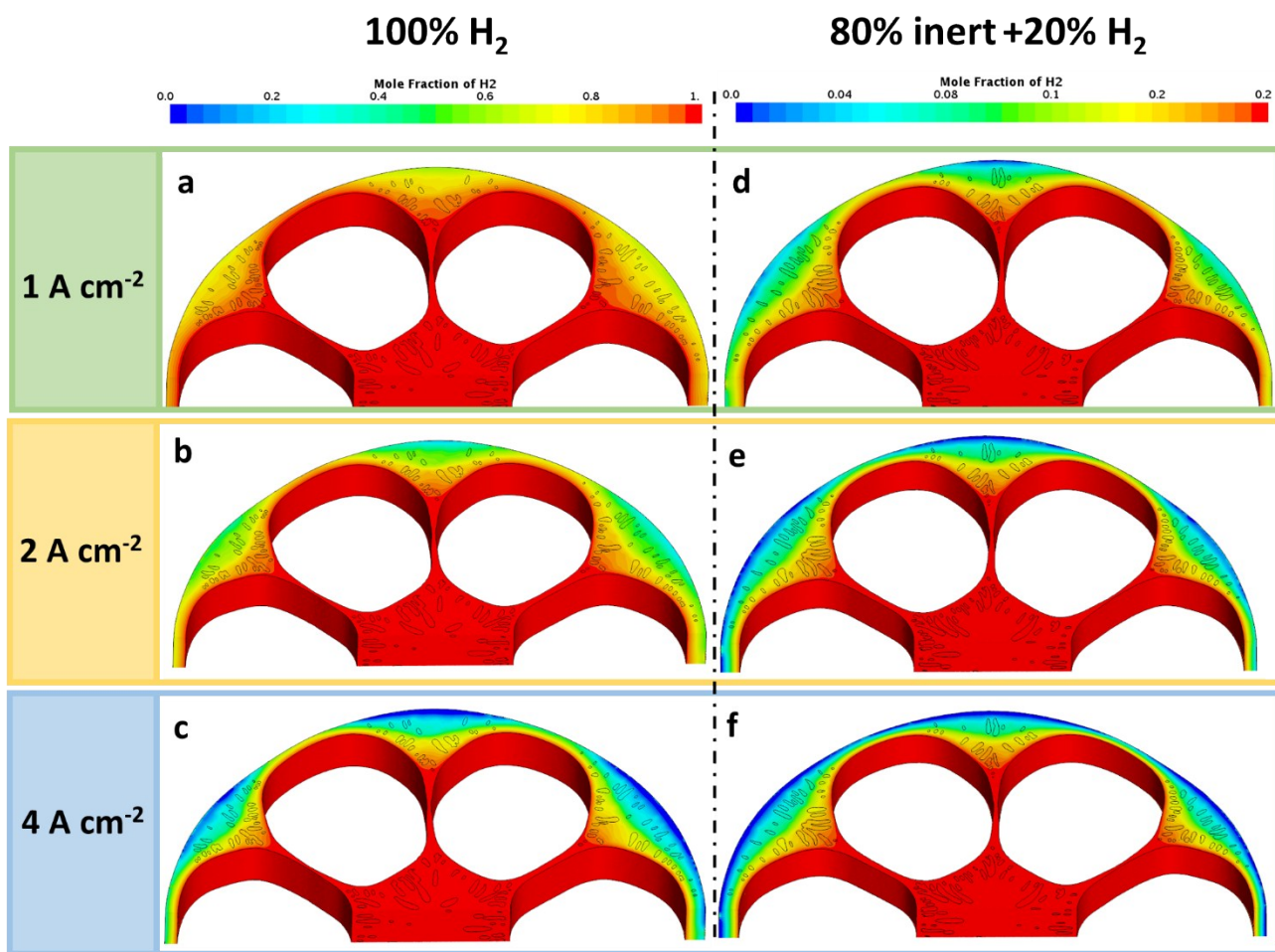
Supplementary Figure 2: Plant layout for ceramic fuel cells operating on LCVGs and air. (HX = heat exchanger and B = blower)



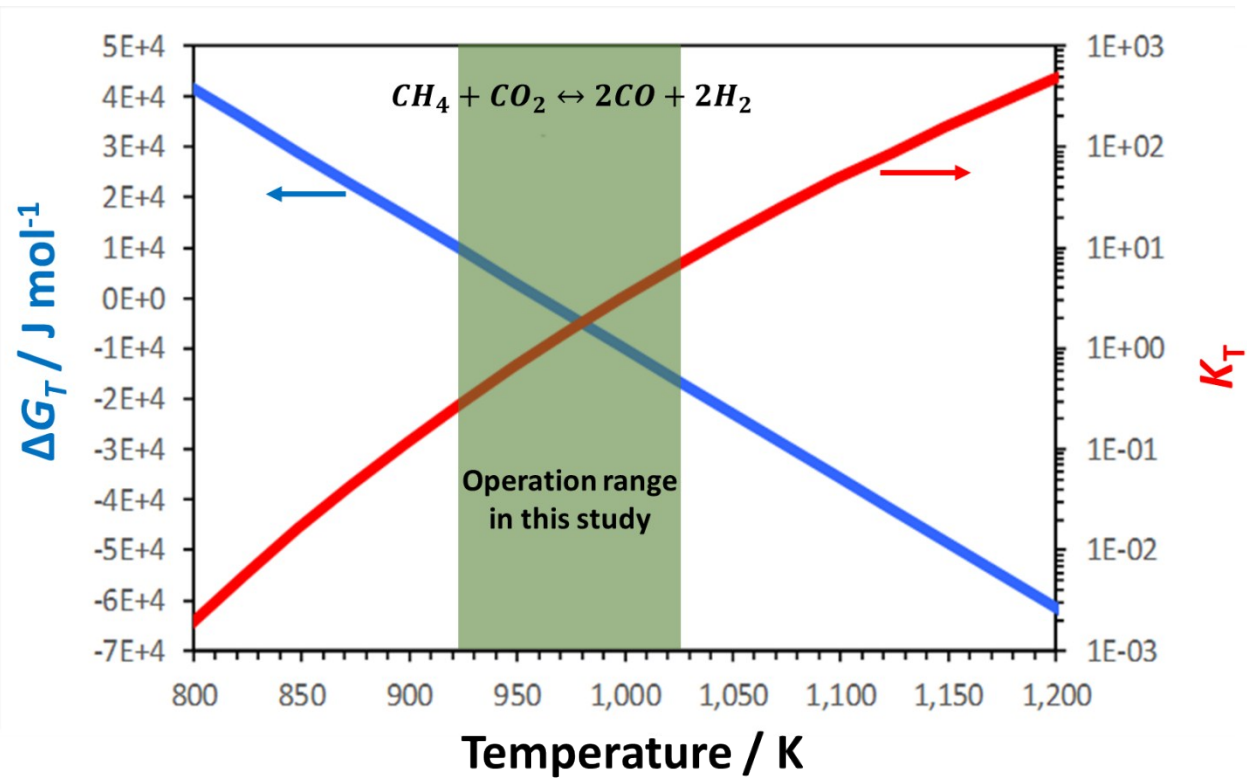
Supplementary Figure 3. SEM photomicrographs of the anode/electrolyte/cathode interface.



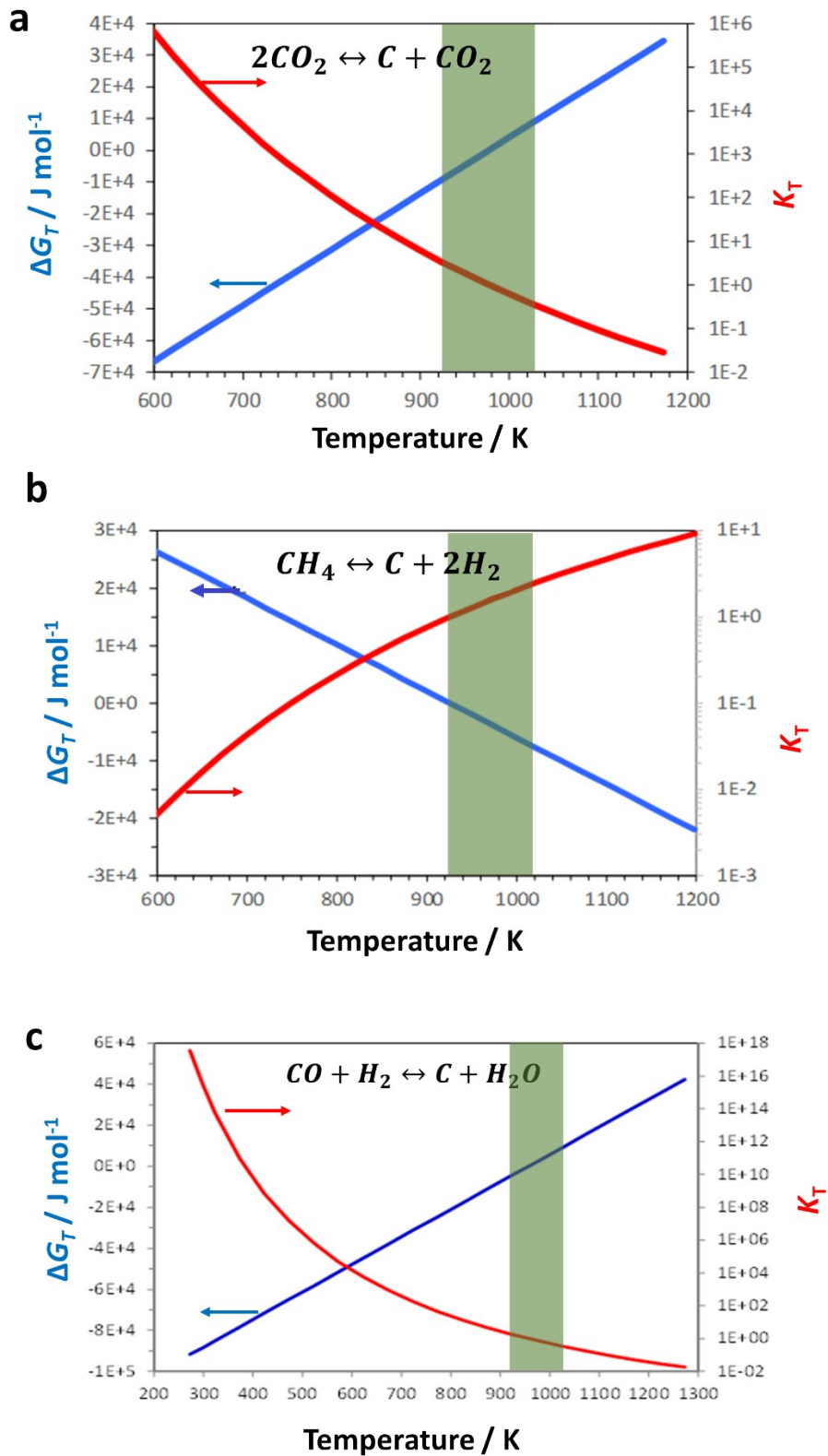
Supplementary Figure 4. Fitted impedance spectra at (a) to (d): 550 to 700 °C with dry H₂ as the fuel and ambient air as oxidant, using the an equivalent circuit $LR_s(R_1||CPE_1)(R_2||CPE_2)$.



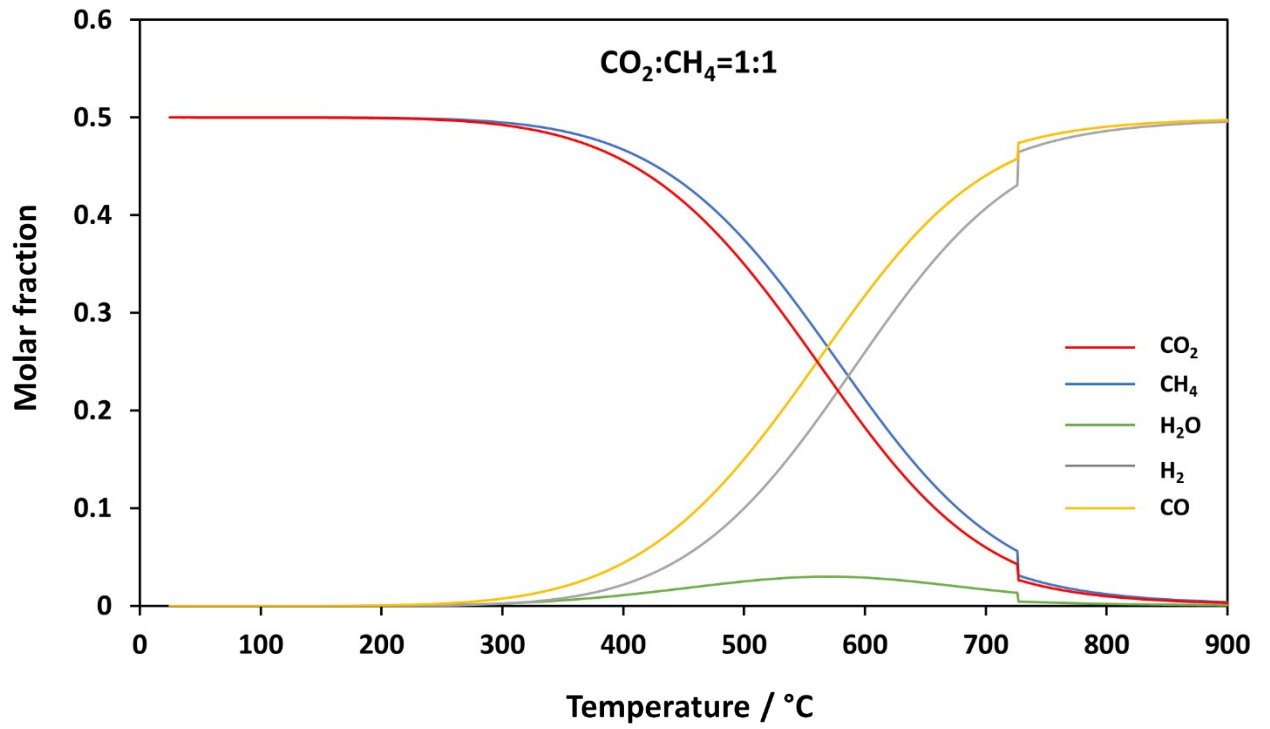
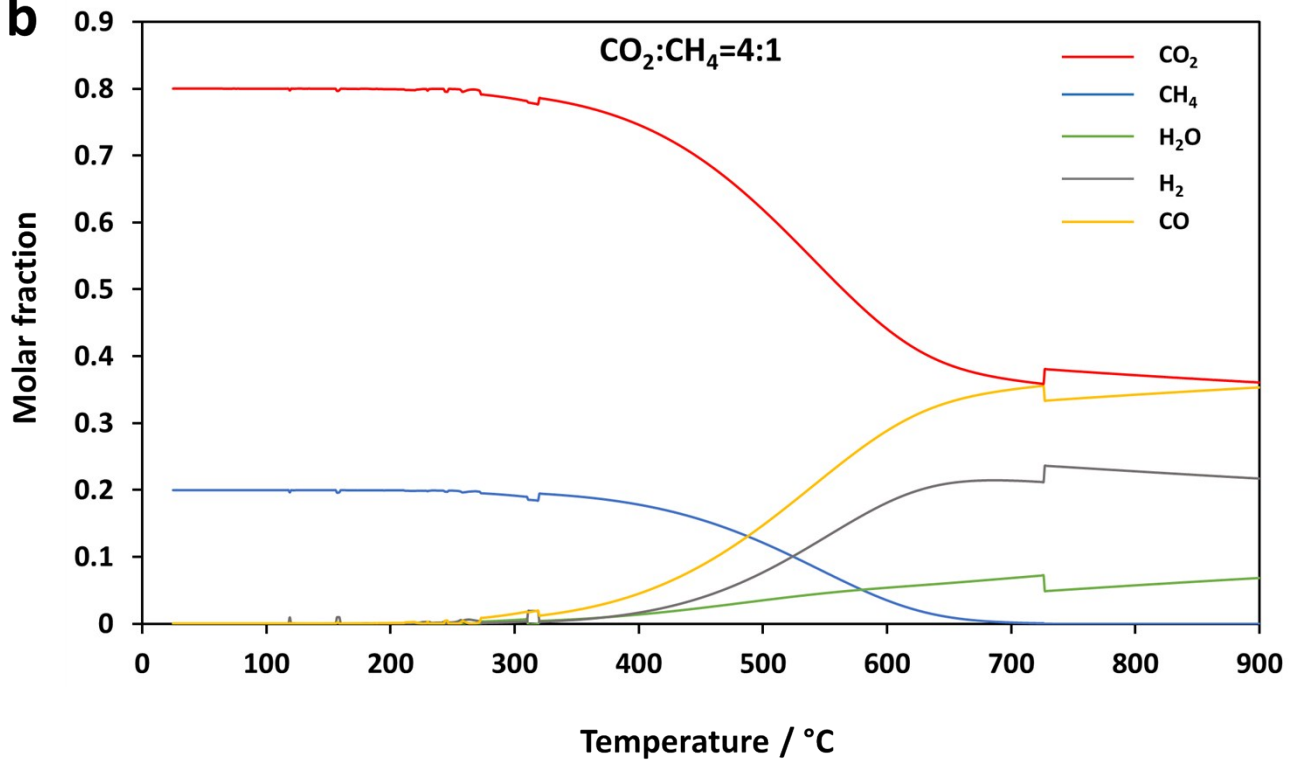
Supplementary Figure 5. CFD modelling of hydrogen molar fraction profile under current densities of 1, 2, and 4 A cm⁻². **a-c.** 100% hydrogen feed; **d-f.** 20% hydrogen feed 80% inert diluent.

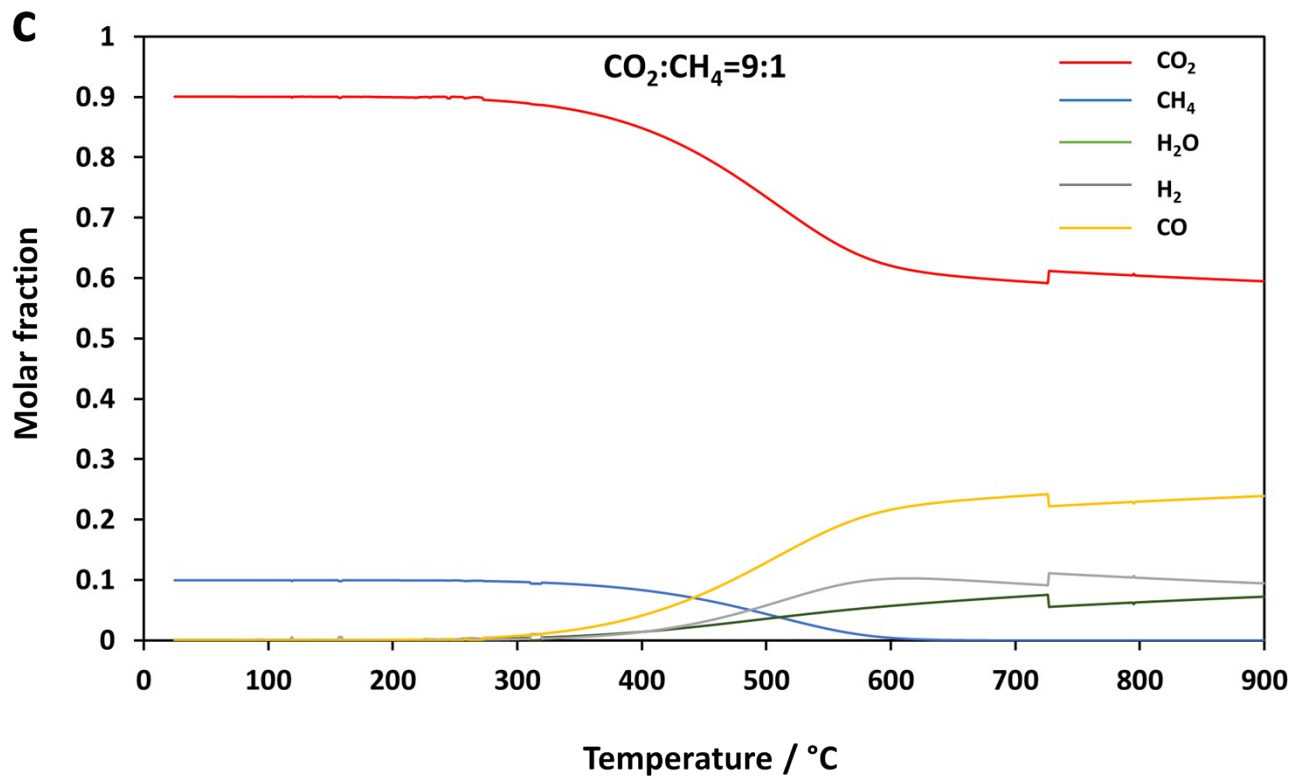


Supplementary Figure 6. (Approximate) Effect of temperature on Gibbs energy change and equilibrium constant (K_T) of DRM reaction

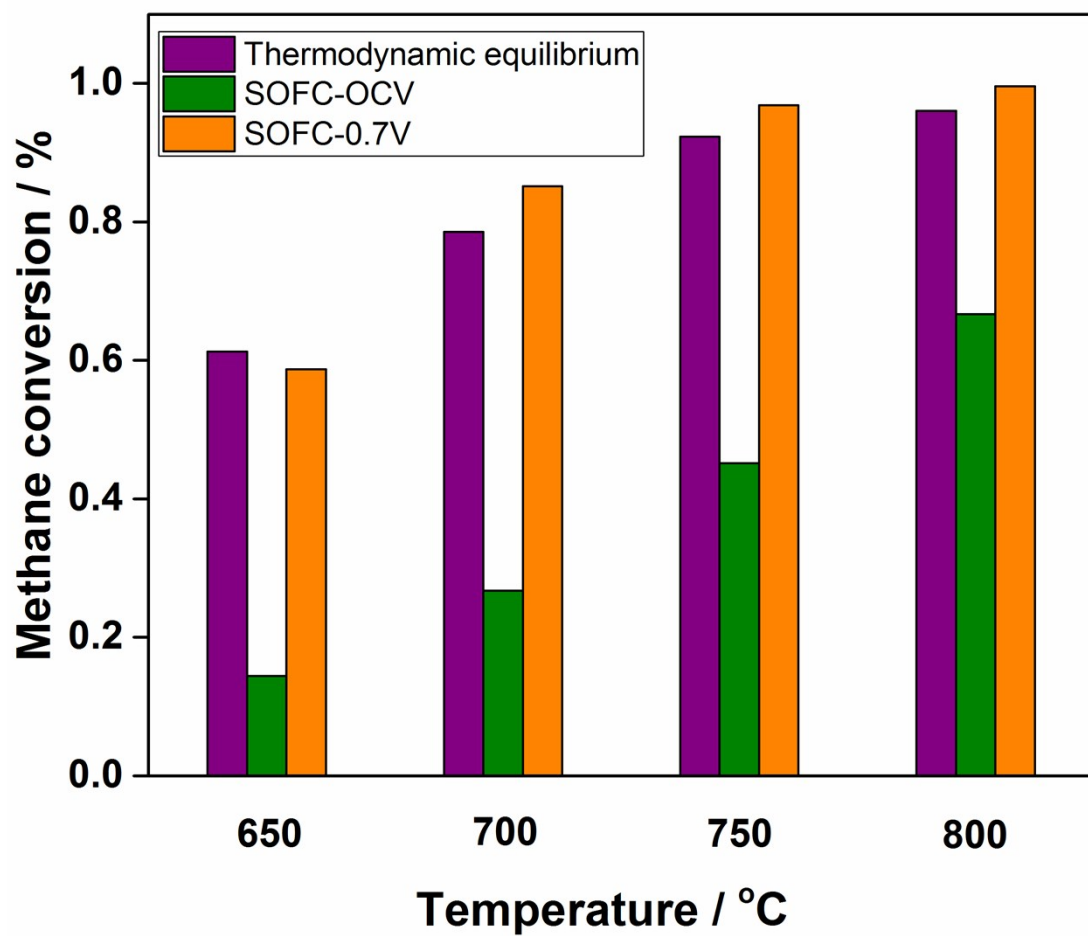


Supplementary Figure 7. (Approximate) Effects of temperature on Gibbs energy change and equilibrium constants (K_T) of side reactions: **a** Boudouard reaction, **b** methane pyrolysis, **c** carbon gasification.

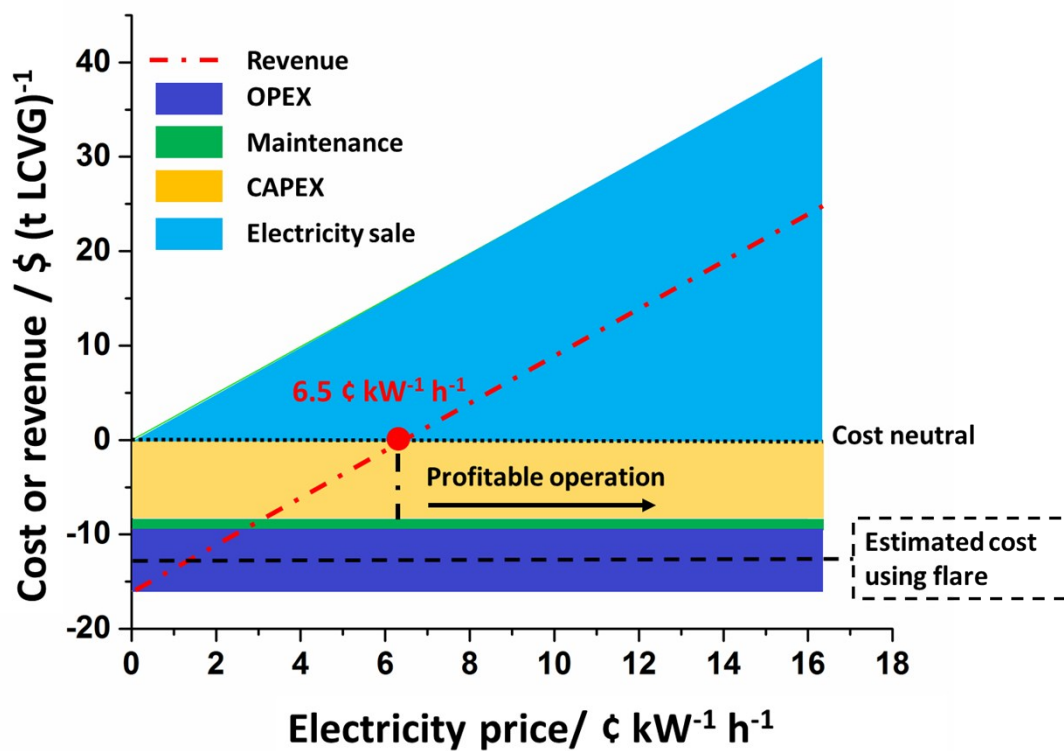
a**b**



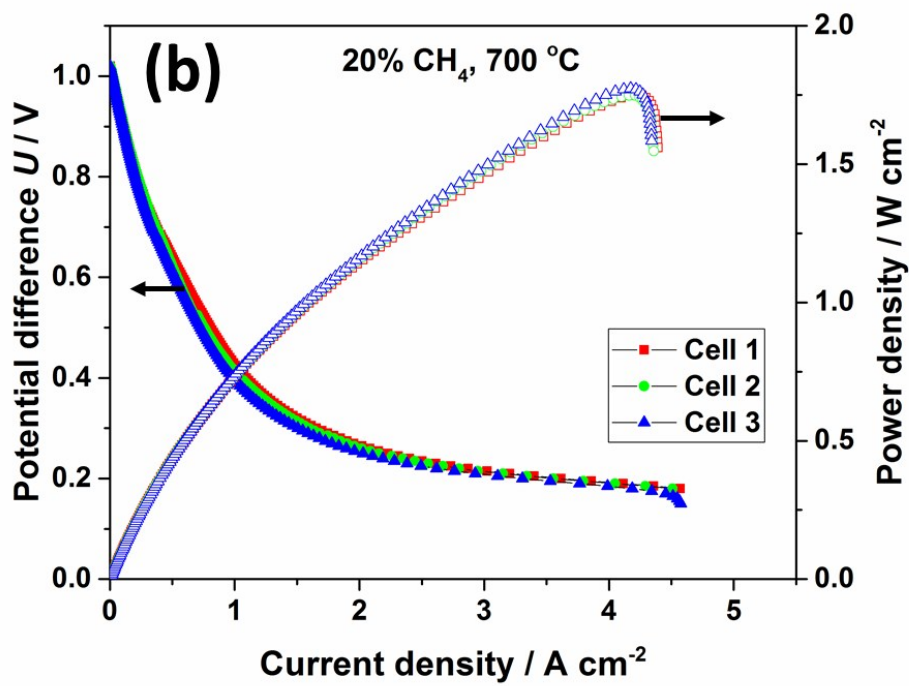
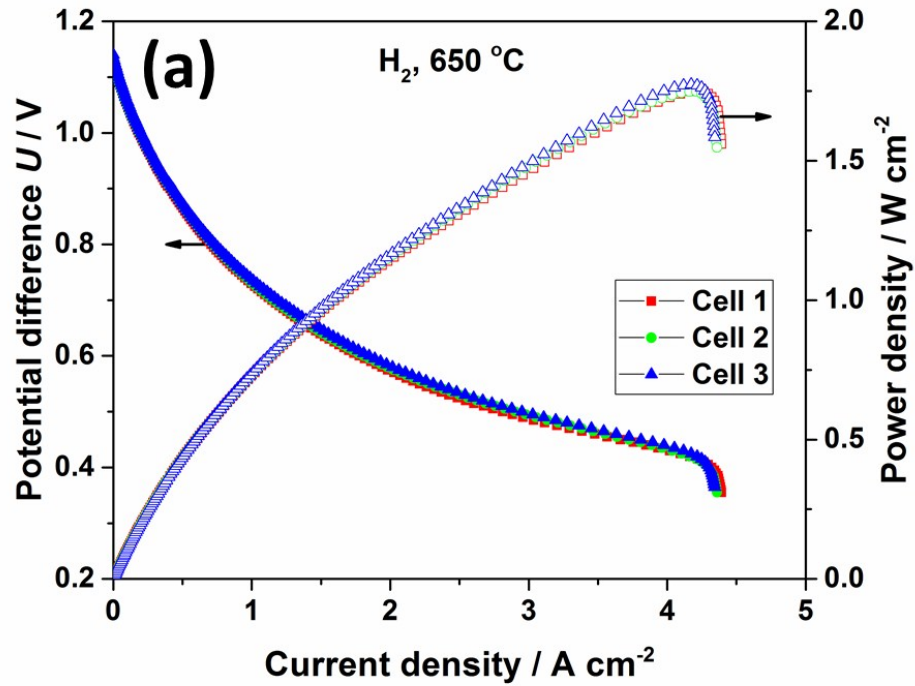
Supplementary Figure 8: Equilibrium composition of CO₂/CH₄ system with **a** 50 %, **b** 20% and **c** 10 % methane concentrations.



Supplementary Figure 9: Methane conversions at temperatures of 650-800 °C from theoretical calculation (purple), open-circuit condition (green) and constant potential difference of 0.7 V, for initial feed composition $\text{CH}_4 : \text{CO}_2 = 1 : 1$



Supplementary Figure 10: Effect of electricity price on profitability for electrical energy generation using ceramic fuel cells fuelled by LCVGs and air as oxidant, operated at 750 °C and 0.75 W cm⁻².



Supplementary Figure 11: j - U curves for three identical cells operated at (a) 650 °C with H_2 fuel and (b) 700 °C with LCVG (20% CH_4) fuel.

Supplementary tables

Supplementary Table 1. Suspension compositions and fabrication conditions of micro-monolithic anode substrates

	Ceramic (wt.%)	66.3 (NiO:YSZ=3:2)
Suspension compositions	Solvent (wt.%)	26.5
	PMMA (wt.%)	6.6
	Additive (wt.%)	0.5
Fabrication parameters	Extrusion rate (cm ³ min ⁻¹)	9
	Bore liquid rate (cm ³ min ⁻¹)	13
	Air gap (mm)	5
Sintering conditions	Temperature (°C)	1400
	Dwell time (h)	6

Supplementary Table 2. The fitted results of EIS in Fig. 2 (b) using $LR_s(R_1||CPE_1)(R_2||CPE_2)$, as the equivalent circuit

Temperature (°C)	Rs (Ω cm ²)	R1 (Ω cm ²)	CPE-T1	CPE-P1	R2 (Ω cm ²)	CPE-T2	CPE-P2
550	0.69	1.53	0.00329	0.65	0.16	0.164	0.92
600	0.37	0.92	0.00347	0.67	0.15	0.139	0.95
650	0.29	0.59	0.00468	0.66	0.16	0.112	1.06
700	0.18	0.40	0.00651	0.65	0.16	0.129	1.06

Supplementary Table 3. Plant Specifications for 4 tonne of LCVG treated per hour

Operating conditions	Values	Reference and comments
Temperature	750 °C	
Cell potential difference	0.75 V	Peak-power density (0.75 W cm ⁻²)
Current density	1 A cm ⁻²	Peak-power density (0.75 W cm ⁻²)
CH ₄ conversion	99 %	
Utilisation of LCVGs	60 %	off-gases are burnt to pre-heat the gases and maintain the temperature within the furnace.
Reactant gases supply temperatures	25 °C	Gases are pre-heated before entering the stack using heat exchangers and furnace.
Pressure	0.1 MPa	
Plant life-time	10 years	With a SOFC stack life of 5 years, operating for 7500 hours a year.

References

- [1] Li, T. et al. A highly-robust solid oxide fuel cell (SOFC): simultaneous greenhouse gas treatment and clean energy generation. *Energy Environ. Sci.* 9, 3682-3686, doi:10.1039/c6ee02562e (2016).
- [2] L. S. Tan. Et al. Removal of high concentration CO₂ from natural gas at elevated pressure via absorption process in packed column. *Journal of natural Gas Chemistry*, 21, 7-10, (2012)
- [3] R. Sinnott and G. Towler, *Chemical Engineering Design*, 5th Edition, Oxford, UK, Butterworth-Heinemann, 2009.
- [4] Matches, 'Matches' Process Equipment Cost Estimates', <http://www.matches.com/equipcost/Default.html> , 2014 (accessed 12/08/2016).
- [5] L. Kleiminger, 'Solid oxide electrochemical reactors and processes for CO₂ and H₂O splitting', Ph.D Thesis, Imperial College London, UK, 2015.